NUCLEAR AEROSOL MEASUREMENT TECHNIQUES

Patrick F. Dunn
Department of Aerospace and Mechanical Engineering
University of Notre Dame
Notre Dame, Indiana 46556

and
Vincent J. Novick
Engineering Division

and

Barbara J. Schlenger
Reactor Analysis & Safety Division
Argonne National Laboratory
Argonne, Illinois 60439

in Advances in Fluid Mechanics Measurements:
Lecture Notes in Engineering, Springer-Verlag, New York, 1988.

NUCLEAR AEROSOL MEASUREMENT TECHNIQUES

Patrick F. Dunn
Department of Aerospace and Mechanical Engineering
University of Notre Dame
Notre Dame, Indiana 46556

and

Vincent J. Novick
Engineering Division

and

Barbara J. Schlenger
Reactor Analysis & Safety Division
Argonne National Laboratory
Argonne, Illinois 60439

Abstract

In this chapter the considerations and techniques used for aerosol measurement in nuclear reactor test facilities are presented. High pressure, temperature, levels of radioactivity and changing chemical composition during this type of experiment impose a number of constraints on the aerosol sampling system. The mechanisms of aerosol formation, transport and deposition within the system are described. The general equations of aerosol transport and deposition are given in detail and are applied for typical reactor aerosol sampling system conditions. The various techniques that could be employed for such systems also are reviewed. Finally, examples of three systems that have been used successfully in large-scale reactor accident experiments are discussed in detail.

Nomenclature

B	Boltzman's constant (1.38E-16 erg/K)
C	Cunningham slip correction factor = $1 + (\lambda/D_p)\ 2.514 + 0.80\exp\left(\frac{-0.55D_p}{\lambda}\right)$
C_p	Gas specific heat at constant pressure
d_w	Wire diameter
D	Diffusion coefficient = $BT\,\tau/m$
D_p	Particle diameter
D_m	Diameter of average mass
D_T	Tube diameter
F	Fraction of aerosol lost or collection efficiency
g	Gravitational acceleration (9.8 m/s^2)
h	STEP channel height
h'	STEP distance between wires
I	Light intensity
k	Coagulation coefficient
K_a	Gas thermal conductivity
K_p	Particle thermal conductivity
Kn	Knudsen number = $2\lambda/D_p$
L	Tube length, path length
m	Particle mass
N	Particle concentration
Pe	Peclet number = Pr · Re
Pr	Prandtl number = $C_p\eta/K_a$
Q	Volumetric flow rate
Q_{ext}	Extinction coefficient
R	Interception parameter = D_p/d_w
R_T	Tube radius
R_b	Radius of bend
Re	Reynolds number = $\rho V D_T/\eta$
Stk	Stokes number (for STEP wire) = $\rho D_p^2 CV/18\eta d_w$
STK	Stokes number (for pipe flow) = $4QC\rho D_p^2/9\pi\eta D_T^3$
T	Temperature
V	Velocity
V_a	Bulk gas velocity in a tube
V'	Gas streamline velocity
V_f	Terminal settling velocity
V_{th}	Thermophoretic velocity
W	Nozzle diameter

δ Skin depth of laminar sublayer

ΔR Radial displacement

∇T Temperature gradient

λ Mean free path of gas molecules

ϕ Angle of bend in radians

η Gas absolute viscosity

ρ Particle density

ρ_g Fluid or gas density

τ Relaxation time = $mC/3\pi D_p\eta$

θ Tube inclination angle in degrees

Introduction

This chapter concerns the methods used to characterize the size, number concentration, radioactivity and chemical composition of nuclear aerosols. From a fluid-mechanical viewpoint, these aerosols can be considered to be a two-phase flow of particles suspended in a flowing gas. In most nuclear aerosol experiments, however, the concentration of particles is not sufficiently high enough to alter the fluid-mechanical behavior of the gas. Yet, on the other hand, the properties of the gas, such as its mean free path, viscosity, and velocity, fundamentally affect many of the ongoing aerosol processes, such as diffusion, impaction and settling. Therefore, it is the fluid mechanical properties of the gas to a large extent that determine the manner in which these particles are to be collected and analyzed.

In the event of a severe accident in a nuclear reactor, a significant portion of the radioactive material available for release to the environment is postulated to be in aerosol form. It is necessary that the nature of these aerosols be evaluated in order for the nuclear community to develop and validate models appropriate for nuclear reactor safety, siting and population exposure analyses. This includes the experimental determination of the amount and timing of their release and their physical characteristics. The latter encompasses their particle size distribution, number concentration, mass concentration, shape, chemical composition and level of radioactivity. This information is essential in determining the transport of material out of the reactor plenum and the deposition and transport through the reactor piping and into the containment building. In order to correctly interpret the aerosol measurements, local thermal hydraulic conditions, including pressure, temperature, flow velocity and gas composition must be known. Data is obtained from experiments that range in size and complexity from bench-scale setups to large tests that are conducted in research reactors.

The focus of this chapter is on aerosol measurement considerations and techniques that are applicable to the large facilities where reactor accident conditions are simulated most closely. Although these considerations and techniques apply directly to the sampling of nuclear reactor accident aerosols, they also relate to the sampling of aerosols formed in other high-temperature and/or high-pressure environments, such as in high-temperature combustion, fires, explosions, etc. The unique features of the reactor aerosol sampling environment are described. The requirements and methodology involved in

developing an appropriate aerosol measurement system are presented. This includes the aspects of both sampling and particle measurement. This chapter does not provide an extensive review of the many approaches that have been taken to sample nuclear aerosols. Rather, it provides examples of several successful systems that have been used.

The foremost consideration in developing an approach to sampling aerosols is first to identify the possible physicochemical nature of the aerosols and their environment. For the case of nuclear aerosols, the nature of the aerosol particles and the gas in which they are suspended depends to a large degree on the type of nuclear reactor being considered. Light water reactors (LWRs), which are cooled with water, are of particular interest, mainly because of their prevalence. Although much of what is contained in this chapter relates directly to aerosol measurements in simulated LWR accident environments, the information is generally applicable to aerosol measurements in other types of reactors.

The accident scenario leading to the formation of aerosols in LWRs can be summarized as follows. The accident is initiated when heat removal from the reactor core is substantially impaired by failure of one or more components in the reactor coolant system. The resulting temperature increase causes the uranium fuel and its cladding to melt. In addition, the cladding can be oxidized by the steam, yielding hydrogen. These processes allow for the release of radioactive fission products from the fuel pellets that are contained within the cladding. Portions of the fuel, cladding, fission products, control rods and structural material in both vapor and aerosol form are carried by the steam and hydrogen from the core to other parts of the reactor and into the containment building from which they may be released to the environment. If the accident progresses far enough, additional aerosol release will result from the interaction of the molten core and the concrete structures below it. However, this chapter deals primarily with aerosol measurements related to the first phase of the accident.

Conditions in experimental facilities where the accident environment is simulated presents the aerosol experimenter with formidible sampling and measurement problems. The pressures can range from 0.2 to 8 MPa, and may vary with time. Temperatures are also high, up to 2500 K, and vary with time and location. The steam-hydrogen gas mixture is chemically reactive and radioactive, primarily due to the fission products that are present in the mixture in both gaseous and aerosol form. The transient nature of the accident results in continuously changing aerosol characteristics. The presence of vapors that can condense onto surfaces or onto existing aerosols rather than directly forming aerosols further complicates the situation.

Ideally, the aerosol sampling and measurement systems should be designed to obtain sufficient information about the aerosols to yield a complete description of their composition, formation, growth, transport and deposition as a function of time and location within an experimental assembly. Such information then would be applied to the understanding of the broader problem of aerosol behavior within an actual reactor undergoing an accident.

Determination of the specific experimental approach to aerosol sampling and measurement depends upon several factors. These include the thermal hydraulic conditions (pressure, temperature and velocity) of the aerosol carrier gas, the anticipated aerosol characteristics such as size distribution, number concentration, chemical composition and level of radioactivity, and the space within and access to the test capsule for instrumentation. These factors primarily dictate the proportion of real-time versus post-test

measurements to be made. Most often, the aerosol measurements are made post-test on the basis of collected samples. This is primarily because more information can be obtained from post-test measurements and because most real-time aerosol measurement systems are relatively complex and are not well suited to operation in severe environments. A majority of measurements are made on samples that are extracted from the flow using a sampling probe. Care must be taken to ensure that the sample is representative and that the aerosol size distribution and composition did not change in transit to the collection device.

In the following sections, specific information related to aerosol sampling and measurement techniques is presented. Examples of several methods are included. These topics are preceeded by a brief description of relevant aerosol mechanisms along with some basic definitions related to aerosol properties.

1.0 Aerosol Mechanisms

The first step in developing an effective approach to sampling and measurement is to identify the mechanisms by which the aerosols are formed, transported and deposited within the reactor containment system.

1.1 Aerosol Formation and Growth

Aerosols can form during a reactor accident by several mechanisms. These include homogeneous nucleation of a vapor, heterogeneous nucleation of vapor onto an existing aerosol (condensation), and fragmentation of liquids and solids. During an energetic core-disruptive accident, aerosols will form by all three of these mechanisms. For most scenarios, however, nucleation and condensation play the most significant role. The process of homogeneous nucleation will form nanometer-sized aerosol droplets. These aerosols will continue to grow by heterogeneous nucleation, yielding droplets in the submicrometer-to-micrometer diameter range. If there is a sufficient quantity of condensible vapor present such that large number concentrations of aerosols are formed (~10^8 particles/cm^3) and if the aerosol transit time through the reactor system is sufficiently long (~1 s), further growth of the resident aerosols can occur by coagulation and agglomeration.

1.2 Aerosol Attenuation

After the aerosols have been formed, there are a number of aerosol attenuation mechanisms that can occur during aerosol transit within the region where the aerosols are formed and within the sampling system that can reduce the aerosol concentration and alter its size distribution. The primary attenuation of the aerosols occurs by their deposition onto structural surfaces. This deposition can occur by impaction, gravitational settling, diffusion, and thermophoresis. Brownian diffusion is dominant for small, submicrometer particles. As the aerosols grow to micrometer size by condensation and/or by agglomeration, gravitational settling and impaction become the dominant mechanisms.

2.0 Extractive Sampling Considerations

Most of the systems used to sample nuclear aerosols are extractive, i.e., they extract or withdraw a "representative" sample of the aerosol from the primary flow for subsequent analyses. These systems typically consist of a probe inserted into the primary flow that extracts a representative sample of particles and gas, a sampling line that connects the probe to the measurement instrumentation and/or collection devices, and a sampling flow control system. In the following, the considerations involved in the development of each of these components are presented. These include a presentation of the methods used to determine (1) the size range of particles travelling upward in the primary flow that will reach the sampling probe inlet, (2) the probe inlet diameter that achieves ideal sampling, and (3) the particle losses that occur in the sampling line during transit to the measurement instrumentation and/or collection devices.

2.1 Particle Transport in Vertical Flow

In most nuclear aerosol experiments extractive samples are obtained from primary flows that travel vertically upward. This is the result of the usual vertical orientation of the fuel pins and control rods. An initial consideration before determining the sampling probe dimensions and its sample flow rate is to estimate the size range of the particles that will reach the elevation at which the probe is located.

The largest particle based on its aerodynamic diameter that can be supported by a given vertical flow can be determined from the Stokes formula:

$$D_p = [18\eta CV)/(\rho-\rho_g)g]^{1/2} \qquad (1)$$

where D_p is the diameter of the particle, η the gas absolute viscosity, C the Cunningham slip correction factor, V the velocity of the gas, ρ the particle density, ρ_g the gas density and g the gravitational acceleration. For the range of pressures and temperatures that are typically of interest, the slip correction factor is near unity except for very small particles (<0.1 μm) and the gas density is small compared to the particle density. As seen in Table 1, only very large particles (supermicron in diameter) travelling with velocities that are typical of the primary flow in a reactor system are too large to be carried vertically upward.

2.2 Sampling Probe Inlet Design

Once the diameter range of particles in the primary flow that can travel upward to the sampling probe elevation is determined, calculations can be performed to arrive at the combination of gas flow rate and probe inlet diameter that provides efficient sampling for all particles of interest. This efficiency is defined as the ratio of the number of particles per unit volume of gas in a given diameter range that is sampled to the number of particles per unit volume of gas in the diameter range that is available to be sampled.

TABLE 1

Maximum Size of a Unit Density Spherical Aerosol Suspended in a Vertical Flow as a Function of Flow Velocity at 2500K

Gas Composition	Flow Velocity (cm/s)	Aerodynamic Diameter (μm)
Steam	3.1	74
	15.7	166
	28.3	233
Hydrogen	2.5	41
	12.4	92
	22.4	124

The behavior of a particle travelling into the inlet of a sampling probe can be evaluated in terms of the particle relaxation time:

$$\tau = mC/(3\pi D_p \eta) \qquad (2)$$

where m is the particle mass. Typical particle relaxation times encountered in a nuclear aerosol experiment are given in Table 2.

TABLE 2

Relaxation Times in Steam or Hydrogen for a Unit Density Spherical Aerosol

	Particle Relaxation Times, τ(s)			
	Steam		Hydrogen	
D_p(μm)	1000 K	2500 K	1000 K	2500K
1	1.52×10^{-6}	5.89×10^{-7}	2.76×10^{-6}	1.49×10^{-6}
10	1.52×10^{-4}	5.89×10^{-5}	2.76×10^{-4}	1.49×10^{-4}
20	6.07×10^{-4}	2.36×10^{-4}	1.10×10^{-3}	5.96×10^{-4}
50	3.80×10^{-4}	1.47×10^{-3}	6.90×10^{-3}	3.72×10^{-3}
100	1.52×10^{-2}	5.89×10^{-3}	2.76×10^{-2}	1.49×10^{-2}

An analysis by Davies (1968) provides an upper and lower limit to the diameter of a small, thin-walled probe that will achieve ideal sampling in still air:

$$s[(2Q\tau)/\pi]^{1/3} < D_T < s^{-1}[(4Q)/(\pi g\tau)]^{1/2} \qquad (3)$$

where D_T is the tube diameter, Q the volumetric flow rate, and s a nondimensional "range limit". Here, a "small, thin-walled probe" is one that has the same sampling efficiency at any orientation. The usual convention for ideal probe sampling is to make the range limit equal to 5. Smaller choices for the range limit result in sampling efficiencies less than 99%. Ideal probe sampling is obtained for a given probe flow rate when D_T is larger than the left side of the equation but smaller than the right side. Sample calculations using Equation (3) and some example sampling conditions are given in Table 3. The ideal sampling criterion is met only for the sizes in the table above the dashed lines. Thus, it is not possible to select one probe size to allow ideal sampling in a still gas for all of these conditions for 20 μm particles using the Davies criterion.

If necessary, a less restrictive criterion may be used to size the probe inlet. Work by Agarwal and Liu (1980) for the case of small, thin-walled probes has shown that a reasonable criterion for still air is:

$$(2\tau^2 g)/D_T < 0.1 \qquad (4)$$

Meeting this criterion gives a still air sampling efficiency greater than 90%. Table 4 provides example calculations for the minimum probe diameter for representative sampling according to the Agarwal-Liu criterion for steam and for hydrogen.

For sampling situations where the primary flow is moving perpendicular (transverse) to the sampling probe inlet, the sampling efficiency can be estimated by [Davies (1968)]:

$$\text{Efficiency} = 1 - 0.8f + 0.08\,f^2 \quad \text{for } f < 1 \qquad (5)$$

where

$$f = [(u^2 + V_f^2)/V_o^2]^{3/4},$$

$$V_o = [Q/(4\pi\tau^2)]^{1/3},$$

and u is the velocity transverse to the probe's inlet axial centerline, V_f the particle terminal settling velocity and V_o the "dynamical sampling" velocity as defined above. This equation gives a sampling efficiency of 90% for 10 μm particles in the case when the transverse velocity is 1 cm/s.

TABLE 3

Probe Diameter (cm) Limits from Davies (1968) Criterion

Steam:				
$Q(cm^3/s)$	1.66	4.2	16.7	16.7
Temperature (K)	2500	2500	2500	1000
$D_p(\mu m)$	Probe Diameter (cm)			
1	.05-12.1	.05-19.3	.1-38.4	.13-23.9
10	.20-1.21	.27-1.93	.43-3.84	.58-2.39
20	.32-.61	.43-.96	.68-1.92	.93-1.20
50	----------	----------	----------	----------
Hydrogen:				
$Q(cm^3/s)$	1.66	4.2	16.7	
Temperature (K)	2500	2500	2500	
$D_p(\mu m)$	Probe Diameter (cm)			
1	0.57-7.52	.08-12.1	.13-24	
10	.27-.76	.31-1.21	.58-2.4	
20	----------	.58-.61	.933-1.21	
50	----------	----------	----------	

TABLE 4

Probe Diameter (cm) based on Agarwal-Liu (1980) Criterion (any flow rate)

$D_p(\mu m)$	Steam (1000K)	Steam (2500K)	Hydrogen (2500K)
1	4.5×10^{-8}	3.6×10^{-9}	4.4×10^{-9}
10	4.5×10^{-4}	36.8×10^{-5}	4.4×10^{-4}
20	.01	1.1×10^{-3}	.01
50	.28	.04	.27
100	4.53	.68	4.35

In general, for primary flow velocities less than approximately a few centimeters per second, a sampling efficiency greater than approximately 90% can be achieved by a probe whose diameter is determined using analyses developed assuming that sampling occurs in "still air", i.e., from a stationary gas with no velocity.

2.3 Transport Losses in Tubes

Once the aerosols have been representatively sampled by the probe, they must be transported with minimal losses to the measurement devices. The ability of a sampling line to transport all particles sizes with acceptably low losses depends upon the settling and inertial effects of the particles travelling in the sampling line, which are dictated primarily by their size and the flow rate through the line. In general, the flow velocity within the sampling line must exceed the settling velocity for the largest particle of interest. However, the flow velocity must not be large enough to cause that particle not to follow its flow streamline and then possibly impact on the sampling line wall along any of its bends. Accepted theories have been developed that account for particle losses during transit as the result of gravitational settling, diffusion and losses in bends for tubes with either laminar or turbulent flow. These are presented below. Existing theory also describes the thermophoretic force on a particle that can occur in a sampling line under certain conditions. This theory, which is used to develop a method for calculating thermophoretic losses in a tube, is presented also.

2.3.1 Gravitational Settling

For laminar flow in a cylindrical, horizontal tube of length L and diameter D_T, the fraction of particles lost is given by Thomas (1958):

$$F_S = 2\pi^{-1}[2Z(1-Z^{2/3})^{1/2} + \sin^{-1}(Z^{1/3}) - Z^{1/3}(1-Z^{2/3})^{1/2}] \qquad (6)$$

where

$$Z = (3V_f L)/4V_a D_T)$$

and V_a denotes the bulk velocity of the gas in the tube.

For turbulent flow, the fraction of particles lost in a cylindrical tube is given by Fuchs (1964):

$$F_S = 1-\exp[-A_g L_d] \qquad (7)$$

where

$A_g = (4V_f)/(\pi V_a)$ is the dimensionless velocity

and

$L_d = L/D_T$ is the dimensionless length

To account for the possibility of an inclined tube geometry, the tube length, L, should be replaced by $L\cos\theta$, where θ is the angle in degrees that the inclined tube makes with respect to the horizontal plane

2.3.2 Diffusion

For laminar flow, the fraction of particles lost in a cylindrical tube is given by Sinclair, *et al.* (1976):

$$F_D = 1 - [0.819 \exp(-3.65\alpha) + 0.097 \exp(-22.3\alpha) + 0.032 \exp(-57.0\alpha) + 0.027 \exp(-123.0\alpha) + 0.025 \exp(-750.0\alpha)] \quad (8)$$

where

$$\alpha = (\pi DL)/Q,$$

D is the diffusion coefficient and Q is the volumetric flow rate.

For turbulent flow, the fraction of particles lost in a cylindrical tube is given by Fuchs (1964):

$$F_D = 1 - \exp[-4V_dL)/(D_TV_a)] \quad (9)$$

where

$$V_d = D/\delta = D/(28.5D_TD^{1/4}Re^{-7/8}(\eta/\rho_g)^{-1/4})$$

and Re denotes the Reynolds number, which is equal to $\rho VD_T/\eta$.

In the region where both settling and diffusion are important, Heyder (1985) provides a method for predicting the total loss from the sum of both effects. The total loss in a tube is given by:

$$F_T = F_S + F_D - (F_D \times F_S)/(F_D + F_S). \quad (10)$$

2.3.3 Bend Losses

For laminar flow, a number of different approaches for bend losses have been taken that all arrive at the same equation. Yeh (1976) transforms the equation to describe the fraction of particles lost in a tube:

$$F_{BL} = 1-2\pi^{-1}\cos^{-1}[(\phi STK)/2] + \pi\sin^{-1}(2\cos^{-1}[(\phi STK)/2]) \quad (11)$$

where the Stokes number is defined in terms of the tube diameter and ϕ is the angle of the bend in radians.

For turbulent flow, the fraction of particles lost in a tube is given by the empirically determined deposition efficiency for a ninety degree bend developed by Pui *et al.* (1987):

$$F_{BL} = 1 - 10^{-0.963STK} \qquad (12)$$

for Reynolds numbers between 1000 and 10,000. The theory of Cheng and Wang (1981) for Re=1000 agrees well with this expression. Calculations using such equations to determine the amount of material lost in a tube bend for angles other than ninety degrees and for Reynolds numbers less than 1000 should be considered to be only estimates. In general, no theory has been able to agree accurately with experimental measurements over the entire flow range that is usually of interest.

2.3.4 Thermophoretic Losses

Thermophoretic losses can be a potential problem for extractive sampling in nuclear systems. Generally, there is a large temperature gradient along the sampling line from the probe inlet to the collection device. Particle deposition onto the sampling line surface due to thermophoresis becomes significant when the ttemperature gradient between the particle and the surface is large and if the particle is small (submicrometer-size). This leads to particle losses along the sampling line.

The thermophoretic force is a force that a particle experiences when it is present in a large temperature gradient. This results from the difference in momentum that arises when "cold" gas molecules strike one of its sides and "hot" gas molecules strike the other side, thereby moving the particle in the direction of decreasing temperature [Waldmann and Schmitt (1966); Brock (1962)]. Particles of diameter $D_p < \lambda$, where λ is the mean free path of the gas molecules, experience a thermophoretic velocity:

$$V_{th} = (-0.55\eta\nabla T)/\rho_g T) \qquad (13)$$

where ∇T is the temperature gradient in the gas surrounding the particle and T is the absolute temperature of the particle. Particles having diameter $D_p > \lambda$ have thermophoretic velocities:

$$V_{th} = (-3\eta CH\nabla T)/(2\rho_g T) \qquad (14)$$

where

$$H = (1+6\lambda/D_p)^{-1}[(K_a/K_p + 4.4\,\lambda/D_p)/(1+2K_a/K_p + 8.8\,\lambda/D_p)]$$

and K_a and K_p are the thermal conductivities of the gas and of the particle, respectively. The mean free paths for the temperatures and pressures typical of reactor tests are on the order of 10^{-2} μm, so that Equation (13) can be applied to only the smallest submicrometer particles.

For laminar flow, the thermophoretic velocity can be used to determine the fraction of particles lost in a tube. The amount of time during which the thermophoretic force is acting is based on the length (or

segment) of the tube, L, over which the wall temperature gradient can be assumed to be constant, divided by the velocity of the flow stream with which the particle is traveling. This force causes a radial displacement, ΔR, from the original trajectory given by:

$$\Delta R = (V_{th}L)/V' \tag{15}$$

where V' is the velocity of the gas along the particular streamline (trajectory). If the particle is initially within ΔR of the wall, then the particle will be lost to the wall before it can leave the tube or segment. The fraction of particles lost in the tube is then given by:

$$F_T = 1 - [(R_T-\Delta R)/R_T]^2 \tag{16}$$

or

$$F_T = 1 - [R_T-(V_{th}L)/V']^2/R_T^2 \tag{17}$$

where R_T is the tube radius.

Figure 1 indicates the dependence of the thermophoretic loss for a typical extractive sampling probe on the thermal conductivity of the aerosol, K_p. For very low particle Stokes numbers, less than approximately 2.5E-5, there is no dependence on K_p. As the Stokes number is increased, this dependence becomes significant. For Stokes numbers greater than approximately 0.04 the % transmission becomes independent of the Stokes number for a given particle conductivity. Figure 2 shows how the type of constituent gas that would be encountered in a typical nuclear aerosol sampling system line affects the quantity of aerosols lost due to thermophoresis.

All the preceeding particle loss equations are derived for monodisperse aerosols, i.e., particles of the same diameter. For aerosol distributions, the loss in each size fraction must be calculated individually. It should be pointed out that a broad aerosol distrubution can give rise to additional mechanisms such as kinetic and thermal coagulation. These mechanisms are important when large differential velocities are developed by the same force acting on masses that are orders of magnitude different. The impact of these mechanisms usually are assumed negligible for reactor aerosol sampling systems because (1) coagulation in the reactor plenum narrows the aerosol distribution , (2) the transport times are rapid, (3) the temperature gradients are reduced, and (4) dilution increases the time between particle collision.

The user of any type of transport system must also realize that while the equations for diffusion and settling are supported well experimentally, the experimental verification for bend losses and thermophoretic losses are practically non-existent. Therefore, it is recommended that a mock-up of any transport system be calibrated experimentally beforehand whenever possible. This will provide the most accurate data for calculating the sampled aerosol parameters from the measured parameters.

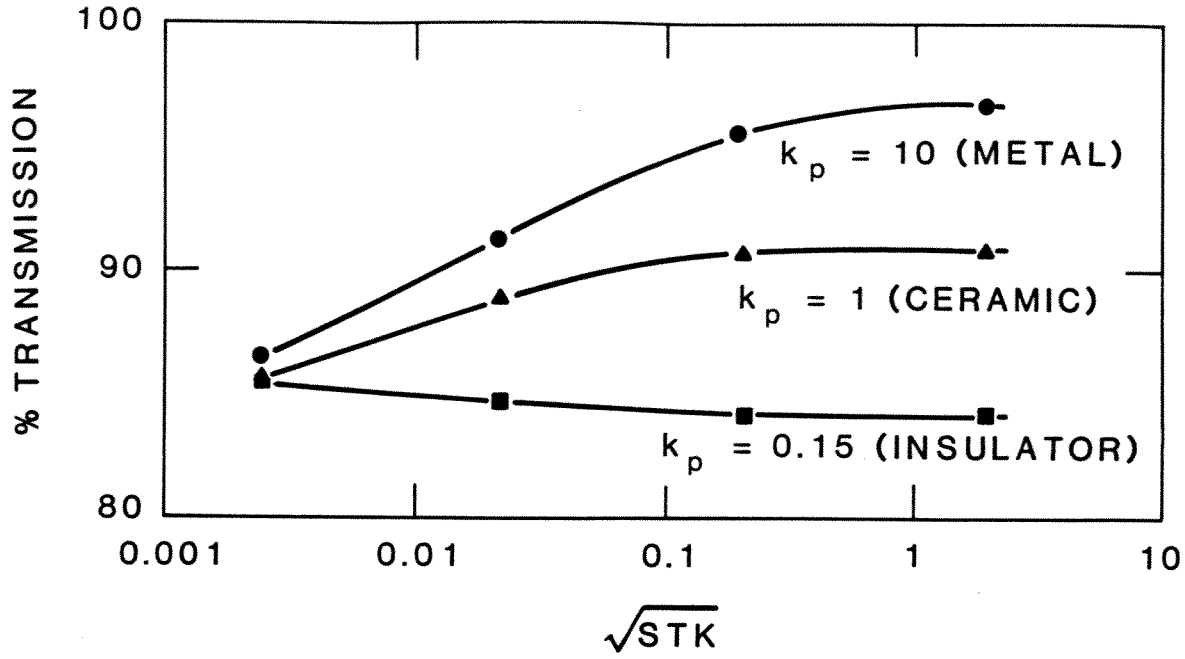

Figure 1. Thermophoretic Loss: Material Dependence

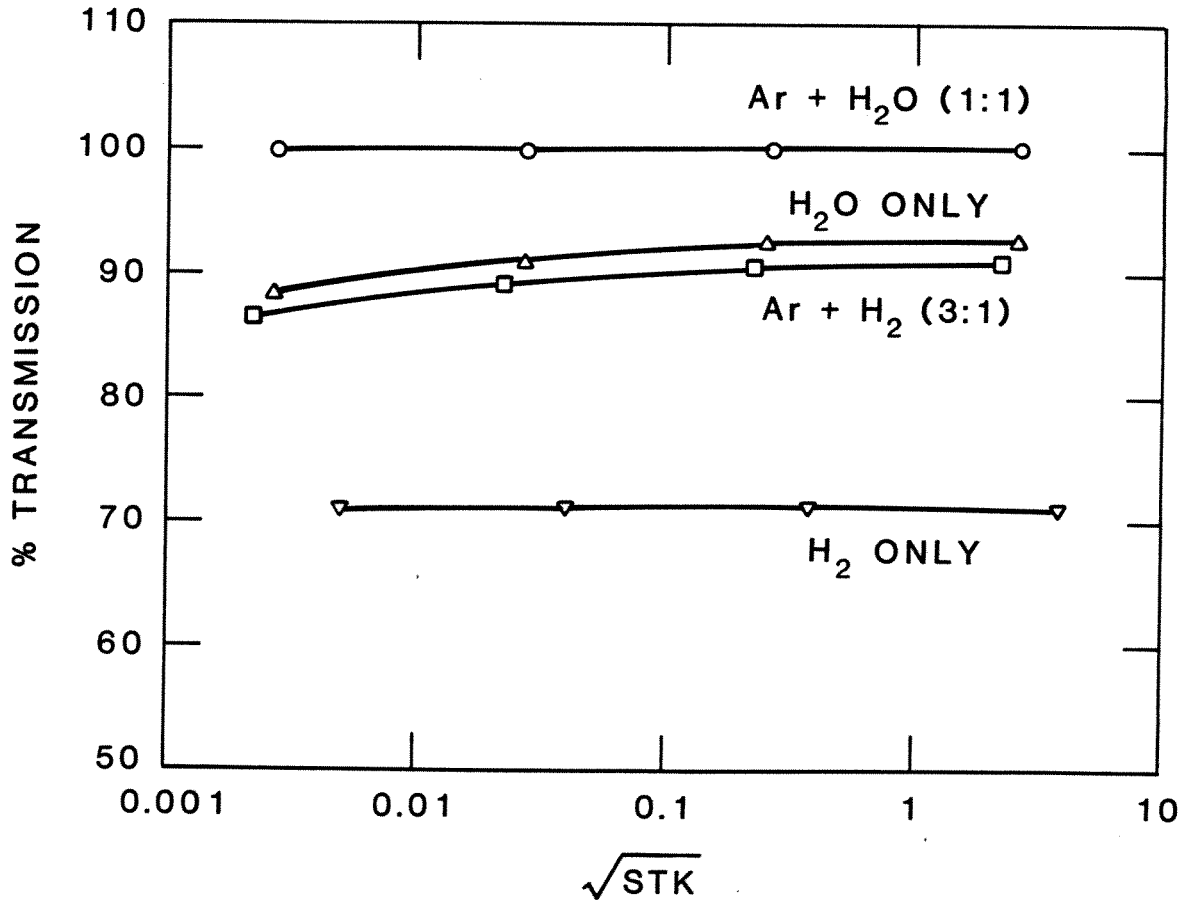

Figure 2. Thermophoretic Loss: Constituent Gas Effects

2.4 Probe Cooling and Dilution

For extractive sampling from nuclear or other high temperature systems, it is an accepted practice to cool and dilute the desired sample with additional gas supplied at the probe tip. This additional gas provides two major functions: (1) it cools the sampled gas rapidly to minimize thermophoretic transport losses and to meet maximum temperature limitations at the collector or reactor seal, and (2) it dilutes the sample sufficiently to 'fix' the aerosol size distribution and number concentration by reducing coagulation effects and eliminating condensation of additional material. Figure 3 gives an example of this type of probe, a variant of which was used in the Loss of Fluid Test (LOFT) experiments [Miller *et al.*(1984); McPherson and Hicks (1986)].

One of the major problems confronting the design of a probe tip is the temperature difference between the sampled gas and the probe sheath or dilution gas. This problem has two facets. One is a materials problem, in that the probe tip must withstand temperatures between 1000 and 2500 K and experience a gradient to approximately 700 K. The second is an aerosol problem, in that the sampled gas moving through the probe tip should not pass a surface cooler than the gas until it mixes with the dilution gas and is cooled by the dilution gas to the probe temperature. This is necessary to minimize the loss of particles by thermophoresis and to prevent possible condensation of vapors. To reduce or eliminate this problem, sheath gas can be introduced into the tip through a cylindrical annulus. The flow rate, tube diameter and cylinder length can be adjusted so that the sheath gas velocity equals or exceeds the thermophoretic velocity. Argon is considered a good choice for sheath gas because it is non-reactive, has high thermal conductivity and has a viscosity near that of steam, which is important for the control of the gas flow.

2.5 Sampling Flow Control System

The primary purposes of a gas flow control system are to control the amount of sample extracted and to provide a constant gas velocity through the aerosol measurement device. This seemingly simple task is complicated because sampling during typical simulated reactor accidents can be affected by changes in the sampling pressure, temperature and gas composition. This is in addition to the materials problems associated with the high-temperature steam that is present in these types of accidents.

These potential problems can be minimized by using a gas flow control system with a critical orifice located downstream of the sampling system that controls the sample flow rate. For this application, the orifice must be sized to allow the desired gas flow into the sampling system to adjust the sampling system pressure so that it is in equilibrium with the pressure of the plenum being sampled. If the size of the orifice is too small, less of a sample will be extracted than desired. If the rate of decrease in pressure in the plenum is sufficiently rapid, then the entire output of the orifice is needed solely to equalize the pressure in the sampling line with the plenum. More rapid rates of pressure decrease will allow only some of the gas contained in the sampling system to flow through the control orifice, while the remainder must flow through the tip into the plenum in order to equalize pressures. For experiments where the rate of change of pressure is known and constant, a properly sized simple orifice will function adequately. If the

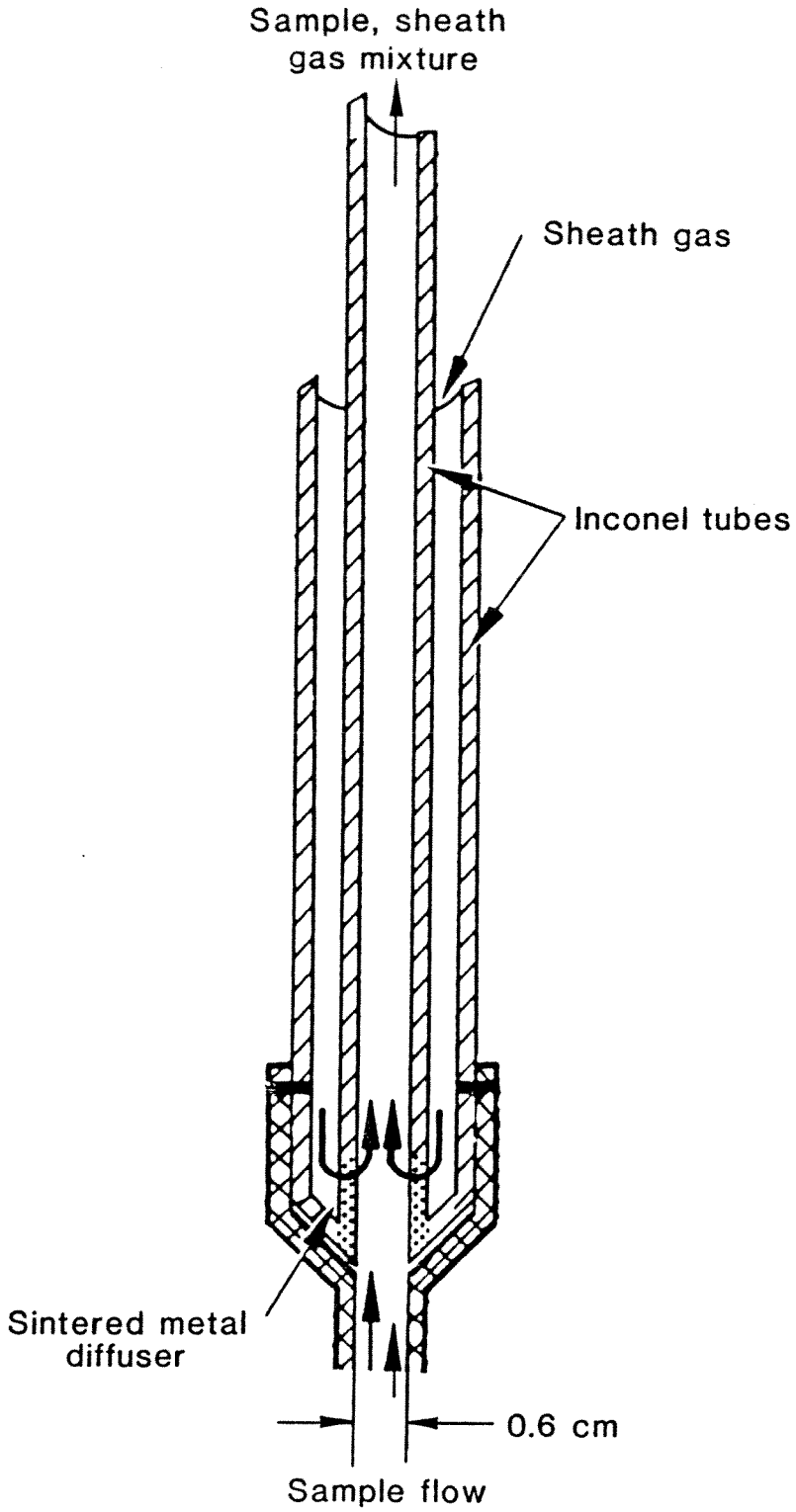

Figure 3. Sampling Probe

rate of change is unknown or not constant, an active pressure feedback mechanism is necessary to properly control the flow.

The use of an orifice also complicates the control of gas flow if the gas composition is changing, even if the pressure remains constant. This is because the gas flow through an orifice is sensitive to changes in the gas constant and specific heat ratios of the gas flowing through it. The specific heat ratio can change by as much as 30% during a typical reactor experiment and the gas constant by more than an order of magnitude. For the specific case of simulated reactor accident conditions, the sampled gas composition changes from steam to hydrogen during the course of the accident. One solution to this problem is to dilute the sampled gas greatly (steam-hydrogen) with another gas such as argon. Unfortunately, too large a dilution ratio results in no control, and thus a considerable uncertainty in the sample gas flow rate.

Another solution to the problem of changing composition is to use a catalyst to change one gas component into another, upstream of the orifice or other control device. For reactor systems CuO can be used as a catalyst to convert H_2 gas into steam. Because this recombination occurs on a mole for mole basis, the volumetric gas flow rate through the orifice remains unchanged. Converting the hydrogen back into steam reduces the impact of varying gas constants and specific heat ratios. Efficient recombination relies on the gas residence time in the recombination chamber and on the exposed surface area of catalyst. Condensation of the steam does not occur because the catalyst recombiner must be heated above 500° C to allow the H_2-to-steam reaction to proceed at a sufficient rate. From an engineering standpoint, the recombiner must be installed upstream of the controlling orifice, but downstream of the particle collection devices. The disadvantage in placing the recombiner downstream of the particle analysis devices is that changes in the viscosity of the gas mixture will introduce uncertainty in the data gathered from these devices. For typical steam-hydrogen-argon mixtures such as those used in the LOFT experiments, the resultant viscosity change was calculated to be less than 20%.

3.0 Aerosol Measurement Techniques

The aerosol measurements techniques that are commonly used in nuclear aerosol experiments are discussed in the following. This section is not intended to be a complete review of all techniques that have been used. Instead, it is intended to provide an overview of the types of systems that are available and how they can be applied for various types of measurements. These measurement techniques are divided into intrusive devices, which are located within the gas flow, and nonintrusive devices, which allow the gas to flow through without obstruction. Mass concentration and radioactivity measurements are emphasized because the goal of nuclear reactor experiments is to determine the total possible mass and activity that can be released for a given scenario.

3.1 Intrusive Techniques

In reactor safety experiments, a considerable number of different techniques have been used to determine the aerosol size distribution and number concentration. These have been primarily extractive,

intrusive techniques requiring post-test analyses. Typically, particles are extracted isokinetically into the sampling system from the flow, i.e., with the same kinetic energy, hence velocity, they had in the flow. Then, they are passed into a collection device that separates the particles according to size by impaction, centrifugal force, gravitational settling and/or electrostatic precipitation. Samples acquired in this manner have often been analyzed to determine the number, mass, shape, chemical composition, and radioactivity of the particles.

Impactors of various designs have been used to measure size distributions over the particle diameter range from approximately 0.5 to 20 μm. These include, for example, size distribution measurements of UO_2, SrO_2 and NaI particles [Sauter and Schutz (1980)].

Spiral centrifuges have been used to determine particle size distributions over the diameter range from approximately 0.1 to 20 μm, including measurements of aerosols produced from simulant nuclear reactor core materials [Albrecht *et al.* (1980)] and of U_3O_8 aerosols [Parker (1980)]. A rotating wheel collection device has been used to determine the velocity and size distribution of aerosols in the 30 to 3000 m/s and 0.003 to 10 μm diameter ranges [Elrick (1980,1982)] produced by neutronically heating fresh UO_2 fuel. Cyclones have been used to size classify aerosols > 1μm diameter [Chyssler *et al.* (1983)].

Elutriators or gravitational settling chambers with collection plates have been developed to size classify simulant reactor core aerosols [Chyssler *et al.* (1983)] and volatile fission product aerosols [Dunn *et al.* (1983)] in approximately the 1 to 100 μm diameter range. Such a device that also incorporates fine wires to collect particles by impaction and diffusion is described in detail in Section 3.5 Another device based upon gravitational settling is a sequentially operated sedimentation sampler [Chyssler *et al.* (1983)].

An electrostatic precipitator has been used to collect yttrium oxide [Kanapilly *et al.* (1980)], sodium oxide and fuel oxide aerosols [Kanapilly *et al.* (1980); Schock (1980)] in approximately the 0.02 to 10 μm diameter range. An electrostatic aerosol analyzer (EAA) and diffusion battery also were used in experiments [Kanapilly *et al.* (1980)], yielding size information in the 0.003 to 1 μm diameter range. Number concentrations of submicrometer-size sodium oxide and fuel oxide aerosols using condensation nuclei counters (CNCs) have been measured, as reported in Nuclear Aerosols in Reactor Safety (1979). Note that the commercially available EAA and CNC devices cannot be adapted to large-scale reactor experiments due to pressure, temperature and gas composition contraints.

Intrusive optical techniques that can charaterize the size distribution of an extracted aerosol include a variety of light-scattering techniques and an aerodynamic particle sizer [Baron (1986)]. An on-line spectrometer also has been patented that can be used to monitor in real-time the size and chemical composition of aerosols [Sinha *et al.* (1982)]. To date, however, none of these optical techniques have been used to sample nuclear aerosols.

The collection of particles onto filters for post-test size distribution analyses has been used extensively. Examples include the collection of PuO_2 and UO_2 aerosols [Bunz and Schock (1979)], simulant reactor core aerosols [Albrecht *et al.* (1980); Chyssler *et al.* (1983)], and fission product and fuel aerosols [Buescher *et al.* (1982); Lorenz *et al.* (1971)]. UO_2 size distributions have also been determined through sieve analysis [Sauter and Schutz (1980)] and collection onto grids for electron microscope analysis [Wright *et al.* (1980)].

3.2 Nonintrusive Techniques

Nonintrusive techniques for particle analysis typically are optical and based upon either imaging or nonimaging techniques. Imaging techniques primarily involve photography of the particles or particle images. Analysis is accomplished following the test. Nonimaging techniques exploit either the extinction or scattering properties of the aerosol. In the former, the attenuation of a light source through a cloud of particles is measured. In the latter, the amount of light scattered from a single or countable number of particles is measured. Scattering techniques require a knowledge of the dependence between incident light wavelength, particle diameter, complex refractive index, scattering angle and polarization. Only in the limits of small or large particle diameter-to-incident wavelength ratios do simple relationships hold. Scattering methods yield a particle size distribution when sufficient parameters are known or measured. They can yield the particle volume-to-surface area mean (Sauter) diameter and number concentration. Also, most scattering techniques are applicable only to particle diameters >0.2 μm. In general, a single extinction measurement yields no information concerning the particle size distribution unless *a priori* assumptions are made about the shape of the distribution.

Forward scattering has been used in the laser aerosol spectrometer for sizing in the 0.4 to 2 μm diameter range [Schock (1980)], and in an optical particle counter in the 0.3 to 25 μm diameter range [Nuclear Aerosols in Reactor Safety (1979)]. The extinction of a single-wavelength HeNe laser light has been used to determine relative changes in the number concentration or mean concentration in sodium mist experiments [Himeno and Takahashi (1980)]. By using two disparate wavelengths of light, the Sauter mean diameter and number concentration can be measured in real-time [Ariessohn *et al.* (1980)]. The extinction method has been used in a series of simulant reactor core experiments [Kanapilly *et al.* (1980)]. This method has been extended by Novick (1988) to using two extinction cells in series to determine the particle number concentration as a function of time, which is discussed in detail in Section 4.4.3. Commercial devices such as a phase/doppler particle analyzer [Bachalo and Houser (1984)] and a particle-counter-sizer-velocimeter [Holve (1986)] may be applicable also. In general, optical techniques are subject to temperature limitations of the window material. Also, electronic components and other materials may be subject to degradation by radiation.

3.3 Mass Concentration

The measurement of mass concentration in reactor safety experiments is best accomplished by the extraction of representative aerosol samples and the subsequent collection in impactors, centrifuges, precipitators, settling chambers or on filters. Post-test analysis (typically weighing) is required for these techniques. The use of filters has been the most frequent approach [Albrecht *et al.* (1980); Bunz and Schock (1979); Buescher *et al.* (1982); Lorenz *et al.* (1971)]. Filter media able to withstand high temperatures include "saffil", an alumina oxide fiber matte, and sintered porous stainless steel. One technique that yields real-time mass concentrations is to direct the extracted aerosol samples onto a piezoelectric crystal microbalance [Woods (1979); Sem and Daly (1979)]. A virtual impactor designed

specifically for mass concentration measurements in a large scale accident simulation experiment is described in Section 3.5

3.4 Radioactivity

Gamma spectrometry can be used in reactor safety experiments to determine the amount and disposition of the condensible and noncondensible radioactive fission products. Both real-time and post-test approaches have been used. For real-time measurements, the aerosol is scanned with stationary Ge(Li) or NaI detectors as it passes them (if there is sufficient activity during transit) or as material is collected onto filters. An on-line fission product detection system has been used to monitor the activity of fission product aerosols [Dunn *et al.* (1983)]. Post-test measurements can be performed after the radioactive aerosols are collected onto filters or other substrates, in condensate traps or in collection tanks. Examples of applying this technique include a system for on-line detection of gaseous and condensed (liquid) fission products during severe fuel damage experiments [Buescher *et al.* (1982)], for on-line detection of corium aerosols [Albrecht *et al.* (1980)], and for post-test determination of fission product and fuel materials [Lorenz *et al.* (1971)].

3.5 Examples of In-Pile Aerosol Measurement Systems

The following systems were designed for use in three different large-scale nuclear accident simulation experiments. They are described in detail in order to provide examples of systems that have been successfully applied for nuclear aerosol measurements. Included with the descriptions are the equations used for their analysis.

3.5.1 The Source Term Experiments Program (STEP)

The STEP experiments consisted of a series of four tests which were conducted in Argonne National Laboratory's Argonne-West TREAT reactor during 1983-84 [Herceg *et al.* (1984)]. The resultant aerosols were collected in aerosol canisters that were designed to characterize the potential releases in both low pressure (on the order of 0.2 MPa) and high pressure (on the order of 8 MPa) environments. Because prior information regarding the characteristics of these aerosols was limited, the system was designed to provide adequate sampling over a relatively wide particle size range. It was also designed to handle a wide range of particle loadings. Two canisters were attached to the STEP experimental test vehicles, as shown in Figure 4. Electrical heaters with temperature-regulated feedback control systems were used to maintain the temperatures of the canisters at the same temperature as that of the primary vessel's upper portion. Signals from the control thermocouples as well as additional thermocouples on the canisters were monitored during each test. The canister entrance ports were located at 0.5 m and 2.1 m above the top of the fuel. These locations allowed for sampling at the minimum and maximum distances above the fuel, given the space limitations of the test vehicles. The canister entrances

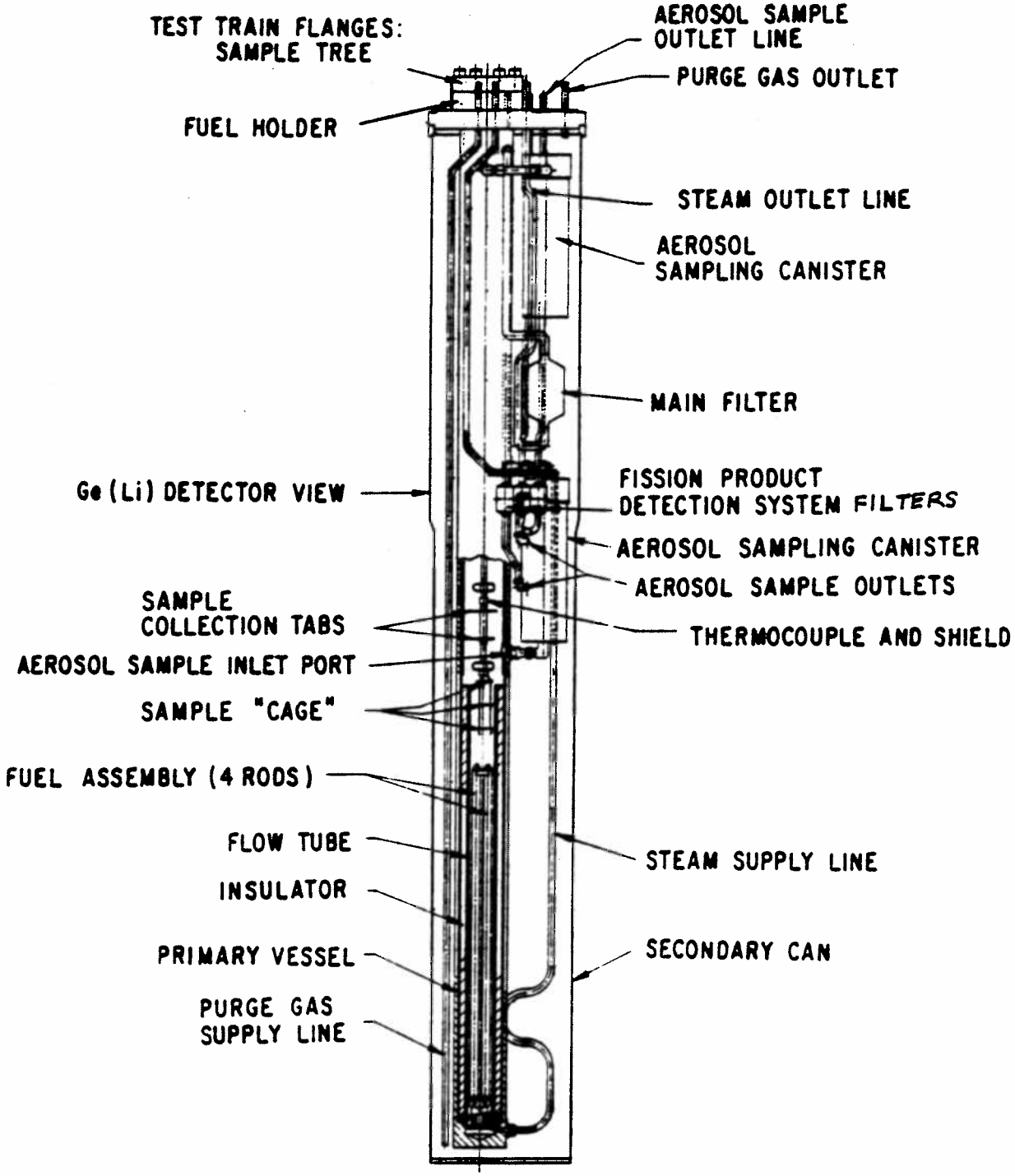

Figure 4. STEP In-Pile Test Vehicle

were flush with the internal surfaces of the primary vessels; space and mobility constraints prohibited extending the sampling lines into the flow streams.

Each canister contained three chambers. Each chamber consisted of a series of stages that were configured in such a way to create a long (3.2m), winding flow channel in a space that was only 0.16 m high. A schematic diagram of the stage arrangement within a canister is shown in Figure 5. Figure 6 shows the stages and collection devices. Significant fractions of the particles were not deposited by impaction around the bends because the velocities were low. The effect on quantitative results by such losses is nevertheless incorporated into the analyses, as described later. The channel cross-section was square. A portion of the steam/hydrogen mixture passed through one or more of the chambers in each canister, and particles were collected on collection devices located in the stages. The individual chambers were exposed to flow during different periods of the tests, allowing for temporal separation of the collected material.

Particles were collected on two types of sampling devices. Settling plates were positioned on the floors of the stages to collect larger particles by gravitational settling and smaller particles by diffusion. Here the chambers functioned essentially as horizontal elutriators. Particles were collected also on wires suspended perpendicular to the flow. The wires collected larger particles by impaction and interception, and smaller particles by diffusion. The system had adequate collection efficiencies for particles over a relatively large size range, from submicron to supermicron in diameter. At least one settling plate and one set of wires were positioned in each stage, with 14 stages per chamber. Therefore, particles were deposited on a large number of collection devices that were positioned along the channel length. Also, because of this 3.2 m long path length, there was sufficient time for many particles to settle gravitationally, leading to a considerable stratification of deposits along the channel length. This allowed for adequate sampling over a wide aerosol concentration.

The settling plates were 0.95 cm square and composed of stainless steel. They were held in position by stainless steel frames that meshed with the walls of the channels. A set of four wires were suspended together on one stainless steel frame, which was identical to the type of frame that supported a settling plate. The wires ranged in diameter from 2.5 to 250 μm (0.1 to 10 mil). These different wire diameters resulted in different collection efficiencies, providing some of the required versatility of the system. The wires were composed of a number of different materials. Most of the wires were chemically inert. Some, however, were not. Therefore, they could react with the fission products and provide information on their chemical composition. In addition, coupons of various materials were attached to selected settling plates to provide additional surfaces for chemical interaction. The material of the stages, entrance tubes, and canister housings was stainless steel.

The collection devices from the canisters were examined post-test using several microanalytical techniques. The purpose of the examinations was to obtain information on the size distributions, morphology and composition of the deposited materials. The majority of the information was obtained by scanning electron microscopy (SEM). The SEM generated images of the collection surfaces. The morphology of the deposits was determined from these micrographs. The SEM was equipped with energy dispersive X-ray analysis capability which was used to identify the elemental constituents of the deposits. Additional chemical and morphological information about the samples was obtained by electron

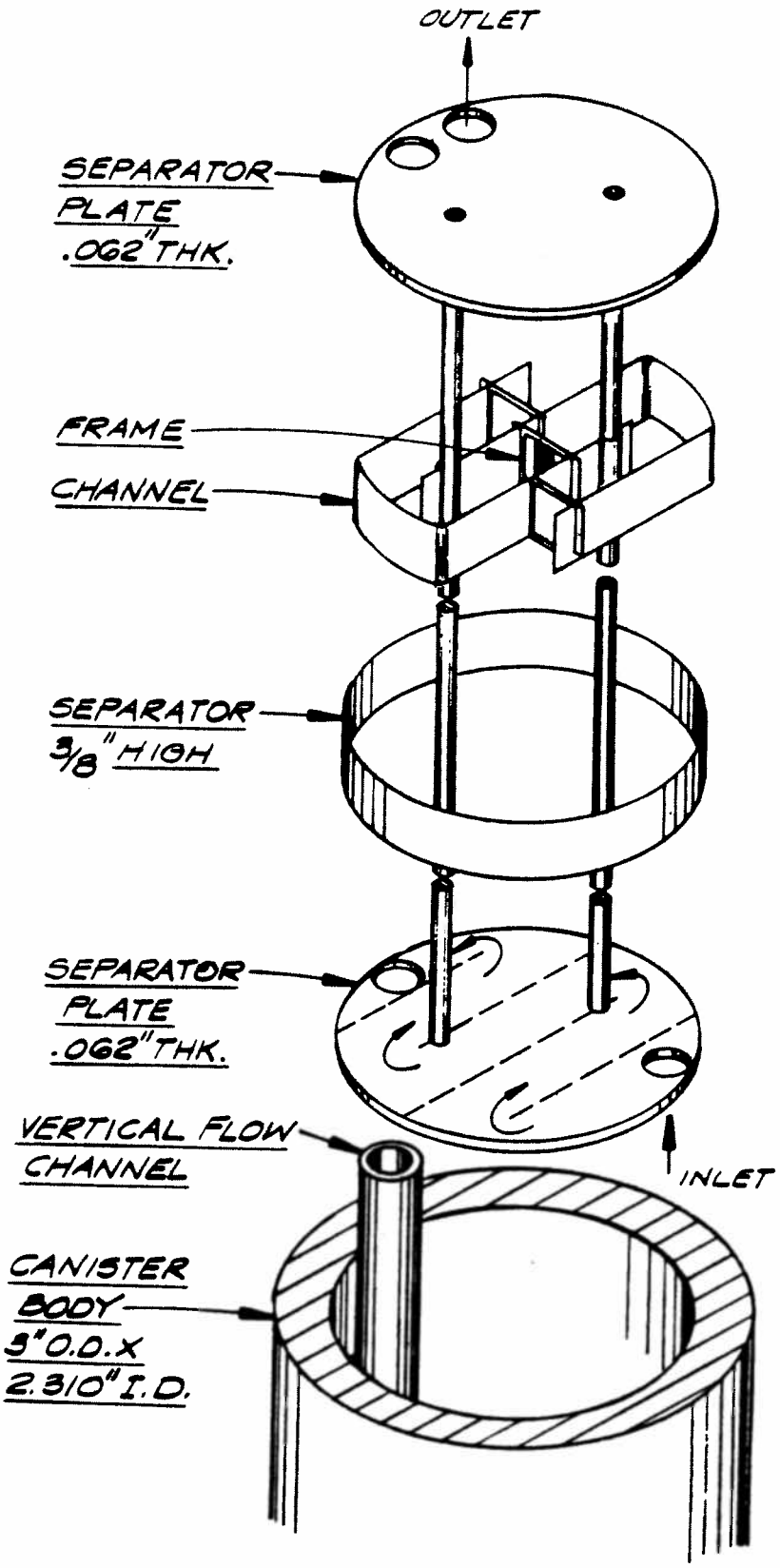

Figure 5. STEP Canister Stage Arrangement

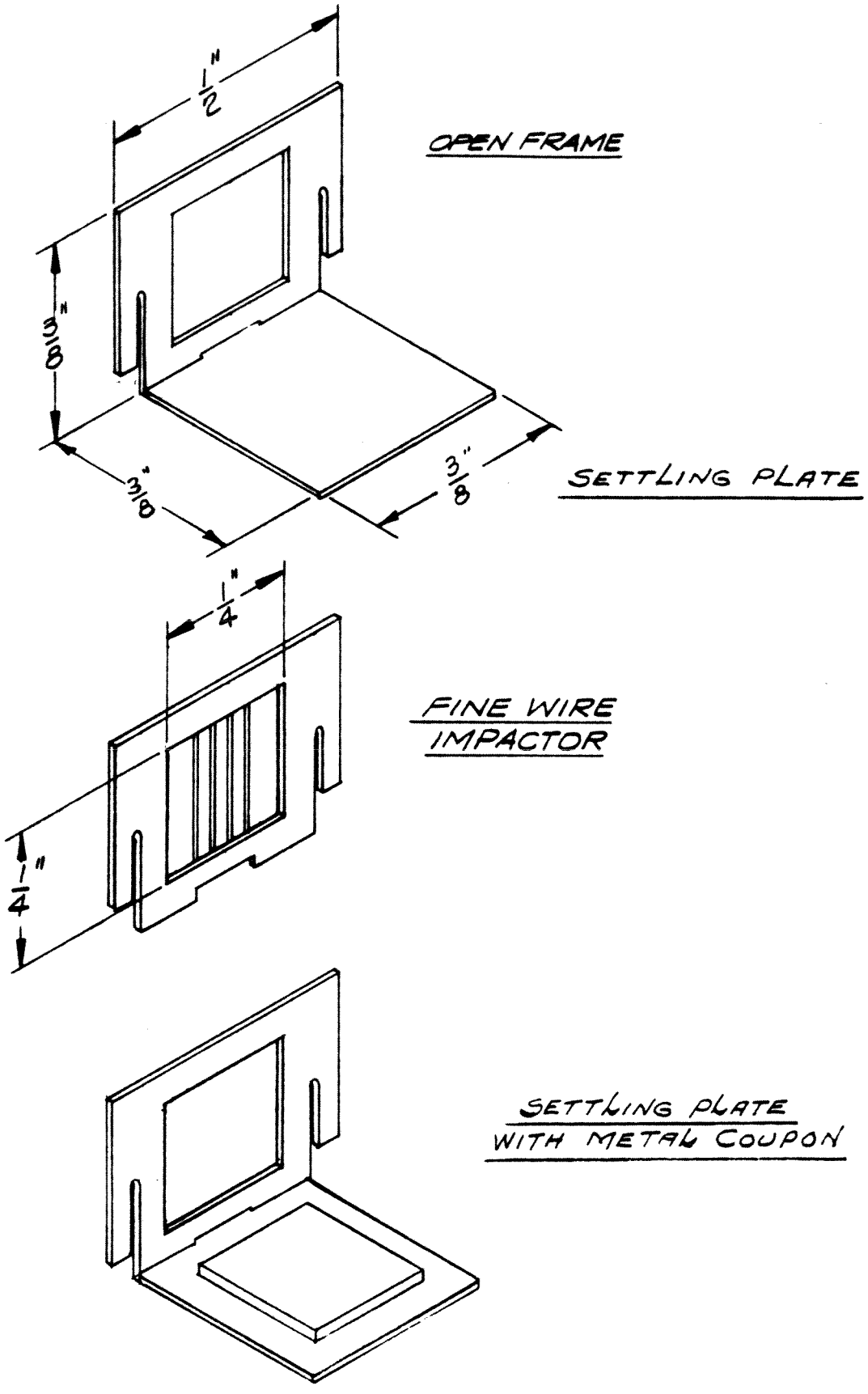

Figure 6. STEP Canister Collection Devices

microprobe analysis, secondary ion mass spectrometry, bulk analysis and X-ray diffraction. There were sufficient numbers of samples to allow for the destructive sample preparation required by some of these techniques.

The procedure for the aerosol size distribution and number concentration analyses consisted first of measuring the diameter of each particle in a selected area on a SEM micrograph and then of sorting the results by size to determine the number of particles in different size ranges on the surface of the settling plate or wire. Collection efficiencies of the wires and plates were calculated for the mean diameters of the particle size intervals using the equations listed below. The collection efficiencies then were applied to the particle count data to calculate the number of particles in the different size intervals that passed the particular collection device. Transport losses in the chamber upstream of the collection device were calculated according to the equations listed below. These losses then were applied to the number of particles that passed by the collection devices, yielding the number of particles in each size interval at the entrance to the chambers. These values were divided by the total gas flow to determine particle concentrations. The particle data was converted to a mass basis using the particle density. The thermal-hydraulic conditions used in these calculations were measured during the tests.

The analysis of the particle data from each micrograph corresponding to collection devices in a particular chamber theoretically should yield the same particle distribution function. In practice, however, there were variations in the results due to nonuniformity in the samples, errors introduced by the particle counting, and the approximate nature of the efficiency equations. By examining many micrographs from different collection devices in a chamber, sufficient data was generated to determine statistically significant values of the distribution functions.

All particles that were deposited were assumed to adhere to the collection surfaces. Forces of adhesion, although difficult to calculate, are known to be strong for particles of the size encountered in these tests. Experience with handling these samples supported the assumption that the material strongly adhered to the collection surfaces.

The collection efficiency equations used in the analysis were compiled from a review of the literature. The selected equations were determined to be the most applicable for the range of flow conditions and system geometry. Although the equations do not exactly model the conditions in the canisters, they are satisfactory, given the required precision of the results. Canister calibration experiments verified the application of the equations selected.

The equations used for calculating the collection efficiency of particles on the settling plates are as follows.

The efficiency of collection by gravitational settling in a rectangular duct is [Ingham (1977)]:

$$F_S = \frac{V_f}{Vh} . \qquad (18)$$

where V_f is the particle vertical settling velocity, V the particle horizontal velocity, and h the channel height.

The efficiency of collection by diffusion is [Ingham (1975)]:

$$F_D = \left(\frac{4}{\sqrt{\pi}}\varepsilon^{1/2} - \varepsilon\right) \cdot 0.25 \text{ for } \varepsilon < 0.02, \tag{19}$$

$$F_D = [1 - [0.694\exp(-5.76\varepsilon) + 0.132\exp(-30.25\varepsilon) + 0.053\exp(-74.8\varepsilon)]] \cdot 0.25 \text{ for } \varepsilon > 0.02, \tag{20}$$

where D is the diffusion coefficient, L the length of the duct, r the radius of the cylindrical duct and

$$\varepsilon = \frac{DL}{Vr^2}.$$

These diffusion equations were developed for plug flow through a duct. Of the geometries for which solutions existed in the literature, this was thought to be the best approximation to the conditions in the chambers.

The total collection efficiency for a plate is approximated by the following equation [Heyder *et al.* (1985)]:

$$F_T = F_S + F_D - F_S F_D/(F_S + F_D) \tag{21}$$

In order to calculate the collection efficiencies of the wires, a model of the flow around the wires is required. This is incorporated into the efficiency equations through the hydrodynamic factor. The hydrodynamic factor, K_H, for a single row of parallel cylinders is [Kirsch and Stechkina (1978)]:

$$K_H = -\ln\left(\frac{\pi d_w}{4h'}\right) - 1.33 + \frac{1}{3}\left(\frac{\pi d_w}{4h'}\right) + \tau Kn, \tag{22}$$

where $\tau \equiv 1$, h' is the distance between wires, d_w the wire diameter and Kn the Knudsen number, which equals $2\lambda/D_p$.

The collection efficiency due to diffusion on a wire is [Natanson (1957); Stechkina and Fuchs (1966)]:

$$F_D = 2.94^{-1/3}Pe^{-2/3} + 0.624Pe^{-1}, \tag{23}$$

where Pe is the Peclet number, which equals the product of the Prandtl, Pr, and Reynolds, Re, numbers.

The efficiency of collection due to interception is [Chen (1955); Kirsch and Stechkina (1978)]:

$$F_R = (2K_H)^{-1}\left[2(1+R)\ln(1+R)^{-1} + \frac{2\tau Kn(2+R)R}{(1+R)}\right], \qquad (24)$$

where R is the interception parameter, which equals D_p/d_w.

A term to account for the combined effects of diffusion and interception is [Stechkina and Fuchs (1966)]:

$$F_{DR} = 1.23K_H^{-1/2}Pe^{-1/2}R^{2/3}. \qquad (25)$$

The efficiency of collection due to impaction is [Brewer and Goren (1984)]:

$$F_{ST} = \frac{Stk^3_{10}}{Stk^3_{10} + 0.77Stk^2_{10} + 0.22}, \qquad (26)$$

where Stk_{10} is defined in terms of the Reynolds number and a function A, where

$$A(K_H,Re) = 4(K_H)^{-1} + 4.95\,(Re)^{1/2}, \text{ and} \qquad (27)$$

$$Stk_{10} = \frac{A(K_H, Re)Stk}{A(K_H,10)}, \qquad (28)$$

where Stk is the Stokes number, defined for this case as $\rho D_p^2 CV/18\eta d_w$. The function $A(K_H,Re)$ was developed for a hydrodynamic factor for a different wire geometry; it is assumed to be valid within the desired accuracy for this application.

The total collection efficiency for wire is approximated by the following sum:

$$F_T = F_D + F_R + F_{DR} + F_{ST}. \qquad (29)$$

The fraction of particles of each size range attenuated by gravitational settling and diffusion along the flow path upstream of a particular collection device were calculated using the same equations as those used for a settling plate, except that the factor of 0.25 in the diffusion equation is neglected (to account for collection on all four surfaces).

The flow passes around a number of 180° bends, n, prior to reaching a collection device. The loss around one bend by inertial impaction is calculated by the following equation [Crane and Evans (1977)]:

$$F_{BL} = \frac{\phi\rho D_\rho^2 VC}{18\eta h}, \qquad (30)$$

where ϕ, the angle of the bend, is expressed in radians.

The total attenuation upstream of a collection device is approximated by the sum:

$$F_T = F_S + F_D + F_{BL} \cdot n \qquad (31)$$

Thermophoretic losses were not considered because the aerosol streams were in thermal equilibrium with the canisters. Electrostatic effects also were not considered because any particle charge would have been neutralized by the ionized atmosphere in the test vehicle produced by radiation and because the canisters were electrically grounded to the reactor structure.

3.5.2 The Loss of Flow Test (LOFT) FP-2 Experiment Virtual Impactor

The sampling and measurement systems for the LOFT FP-2 experiment [McPherson and Hicks (1986)] are shown schematically in Figure 7. In this experiment the aerosol mass concentration was determined using a virtual impactor. This type of impactor, like the cascade impactor, uses inertial impaction to size classify particles. Cascade impactors are probably the most widely used devices that seprate particles according to their aerodynamic particle size. Cascade impactors can be designed for a wide range of flow rates, pressures, and temperatures, providing particle classification for up to 20 size ranges. Major drawbacks to cascade impactors are particle bounce and the limited amount of mass that can be collected on each substrate.

The virtual impactor is a device that allows particles to impact upon a void rather than a substrate while maintaining a minor flow through the void. Virtual impactors size particles by directing a particle-laden gas jet toward a collection probe that allows only a small fraction of the flow of the impinging jet to pass. This forces a majority of the flow to turn and exit the probe. The larger particles cannot negotiate the turn but follow the minor flow in the probe and are carried to a collection device. The smaller particles follow the streamlines of the major flow and are collected separately. A multistage impactor iterates this process with the major flow within practical limits.

A virtual impactor does not suffer from particle bounce, and the sample is collectecd by filtering the major and minor flow, thus collecting larger amounts of mass than a cascade impactor given the same external dimension. Internal losses are typically greater in virtual impactors, and the larger particle size fraction contains a percentage of the small particle size fraction roughly equivalent to the percentage of minor flow. The traditional virtual impactor separates particles into only two size ranges. The device developed for the LOFT experiment consists of a two-cut point, three-collectable fraction virtual impactor [Novick and Alvarez (1987)]. This device retains the advantages of large mass collection and reasonably sharp cut points while providing definition of particle size distribution via the three size ranges. The small physical size of the impactor permits its application to a variety of environments.

The two-stage impactor is shown in Figure 8. It was designed to be small in size and to handle a 2 L/min flow rate. The minor flow through most virtual impactors ranges between 5 and 15%. However,

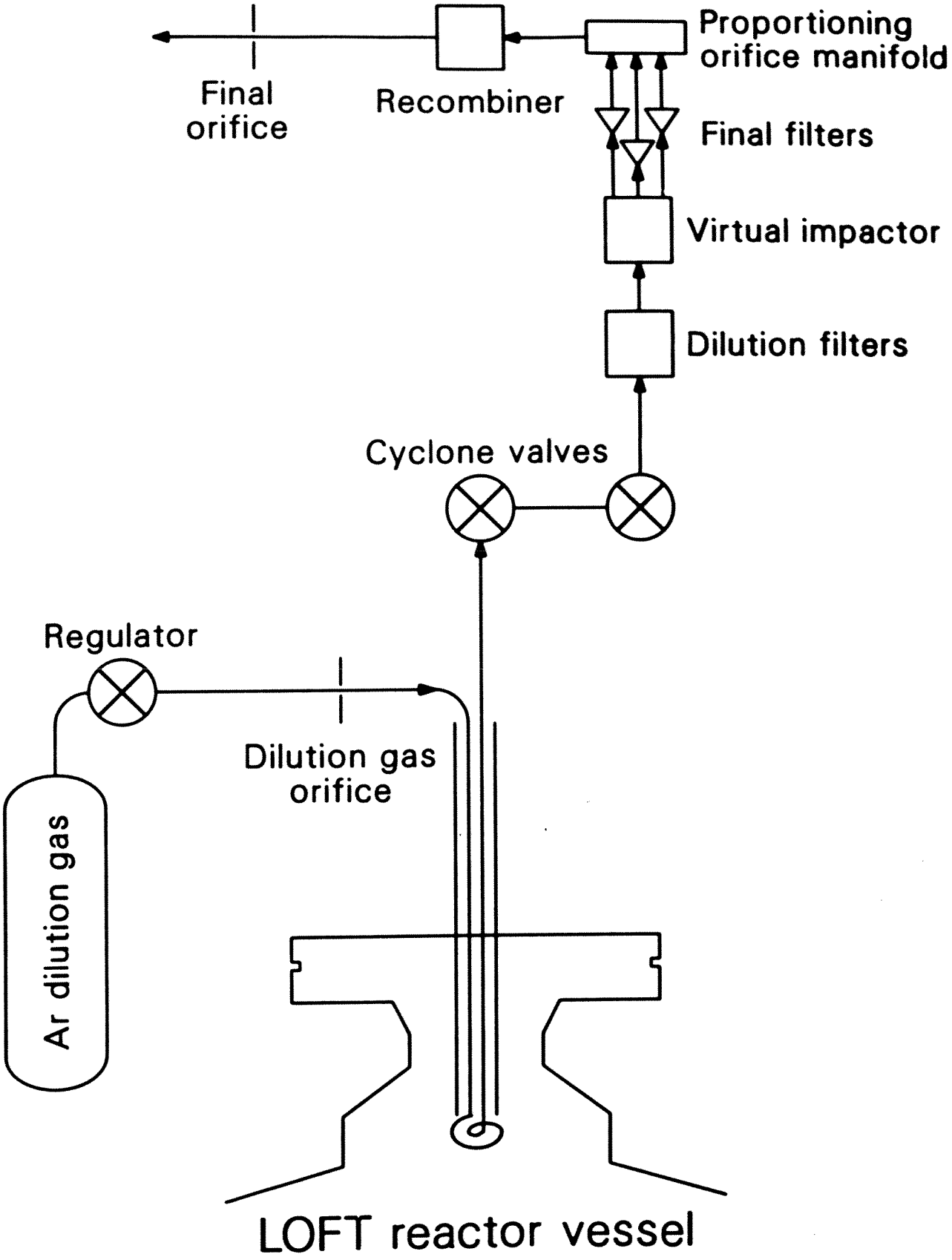

Figure 7. LOFT FP-2 Sampling System

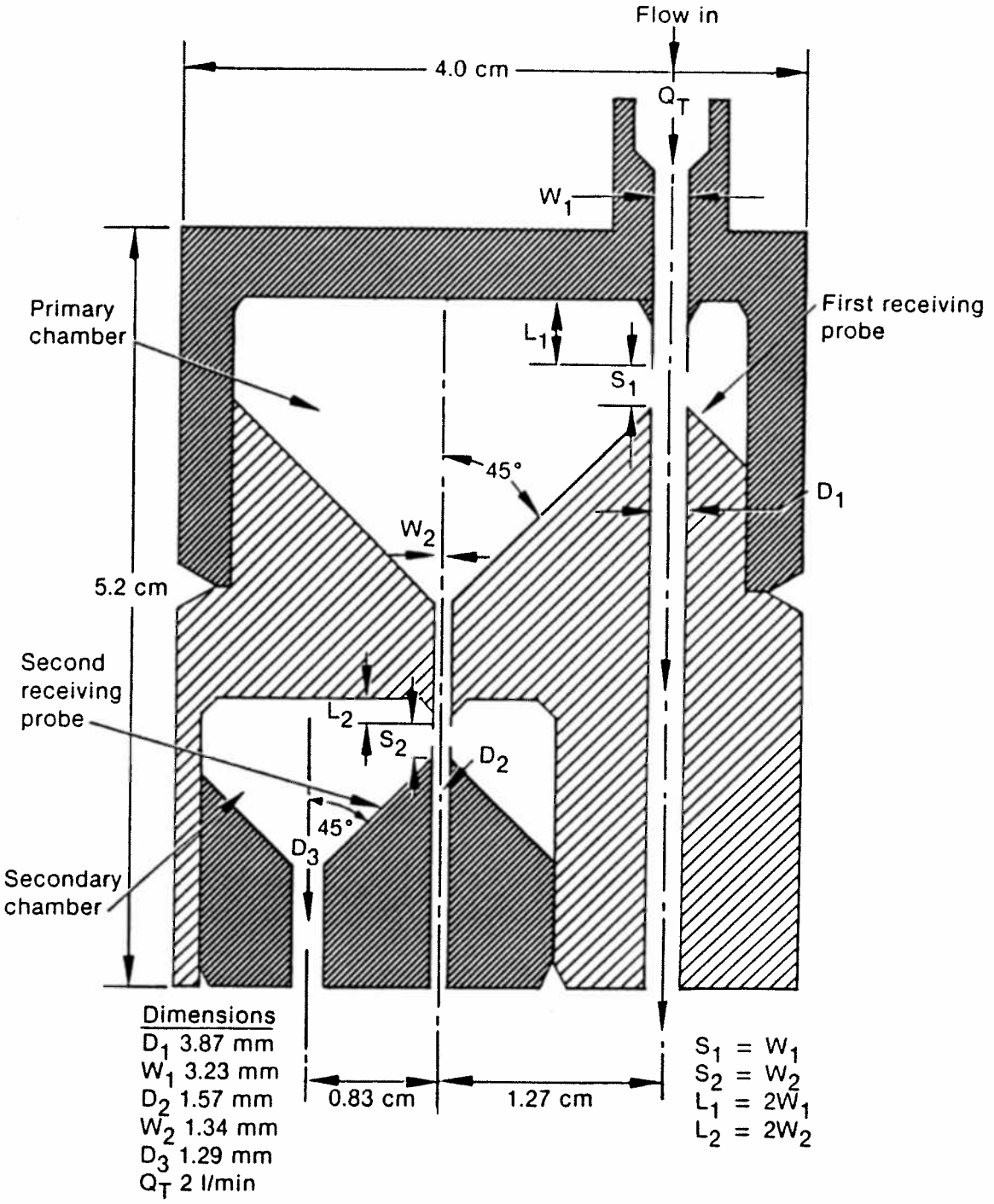

Figure 8. Two-Stage Virtual Impactor

this prototype was designed for minor flows between 15 and 20% in order to keep particles larger than 15 μm suspended in a vertical upward flow, required by the experiment for which the impactor was originally designed and tested. At this flow rate and a nominal temperature of 650 K, the first stage cut point occurs near 10 μm and the second stage cut point is near 3 μm. Flow through each stage is controlled by an orifice. The sum of the orifice areas can be used to control the total flow rate, Q, through the impactor, while the ratios of the orifice areas are used to control the relative amounts of major and minor flows. Filters are placed upstream of the orifices to collect the three particular size fractions. The operating characteristics of the impactor are governed by the Stokes number:

$$Stk = \frac{4pQCD_p^2}{9\pi\eta W^3} \tag{32}$$

where the characteristic dimension is the diameter of the nozzle, W, for a given stage.

A virtual impactor allows a fraction of the total flow to pass through the inlet probe of each stage. This fractional flow transports the larger particles to a collector but also entrains a fraction of low inertia particles (those smaller than the cut point diameter). This results in an efficiency curve that does not approach zero for sufficiently small values of particle Stokes number as do efficiency curves for cascade impactors. Virtural impactor efficiency curves instead approach a value based on the precentage of flow through the separating stage. This requires a correction to be applied to the values of the mass sampled by each stage to give the actual mass in the particular size class. The first-order corrections to the measured mass in each size class for a two-stage impactor are given below. If x, y, and z are the measured values of the collected mass, and X, Y, and Z are the corrected values for size classes X, Y, and Z, then:

$$Z = \frac{z}{1-q_1-q_2} \tag{33}$$

$$Y = \frac{y - q_2 Z}{1-q_1} \tag{34}$$

$$X = x - q_1(Y+Z) \tag{35}$$

where q_1 is the fractional flow through the first stage, q_2 the fractional flow through the second stage, X and x the first stage values, largest class size, Y and y the second stage values, middle class size, and Z and z the third stage values, smallest size class.

Experimental laboratory testing has confirmed that the virtual impactor is able to accurately describe particle size distributions by determining the mass mean aerodynamic diameter and the geometric standard deviation. The impactor operates at close to theoretical efficiencies and sharpness of cut points. The

prototype routinely collects 20 to 40 mg of aerosol mass with the total internal losses less than 9%. The impactor is extremely versatile. A wide range of cut points are available with a single design by simply changing the flow rate through the impactor.

3.5.3 The Power Burst Facility (PBF) SFD 1-4 Experiment

Most optical aerosol monitors for reactor experiments only measure the extinction of a beam of light. The extinction measurement can be interpeted as a history of the mass flux of aerosols during the experiment if both a particle size history and extinction coefficient history are assumed. A similar extinction device was added to the PBF SFD 1-4 experiment, as is shown in Figure 9. A schematic of the aerosol sampling and measurement systems for the PBF SFD 1-4 experiment [Adams *et al.* (1986); Osetek (1987)] is shown in Figure 10. This device differed from other extinction measurement devices by using two extinction cells in series. For sufficiently high concentrations of aerosols, a difference in the extinction between the two cells can be detected and explained by coagulation, which tends to decrease the total cross-sectional area of the aerosol in the second cell, hence reducing the amount of extinction [Novick (1988)].

For a polydisperse aerosol, the extinction coefficient, Q, must be written as an integral over particle size, particle extinction coefficient, and size distribution. Let the value of this integral be designated by Q_{ext}. An equation describing the light extinction can be written for each cell. Hence,

$$I/I_o = \exp[-N\pi D_m^2 L Q_{ext}/4] \qquad (36)$$

and

$$I'/I_0 = \exp[-N'D'^2_m L'Q'_{ext}/4] \qquad (37)$$

where N is the particle concentration, D_m the diameter of average mass, L the path length, I the measured light intensity and I_o the intensity of the light incident upon the particles. The unprimed and primed designations denote the first cell and the second cells, respectively. Because the cells are in series, the transit time is short, and therefore Q_{ext} equals Q'_{ext} and D_m equals D'_m. These assumptions are valid provided the coagulation process does not appreciably increase the particle size. D_m is used instead of the geometric size to describe the particle size because the total mass remains constant. Using the above assumptions and dividing Equation (37) by Equation (36) the following equation is obtained:

$$\frac{\ln[I/I_o]}{\ln[I'/I'_o]} = \frac{LN}{L'N'} \qquad (38)$$

This equation is dependent only on the measured values of the intensity ratios for each cell and the number concentration in each cell.

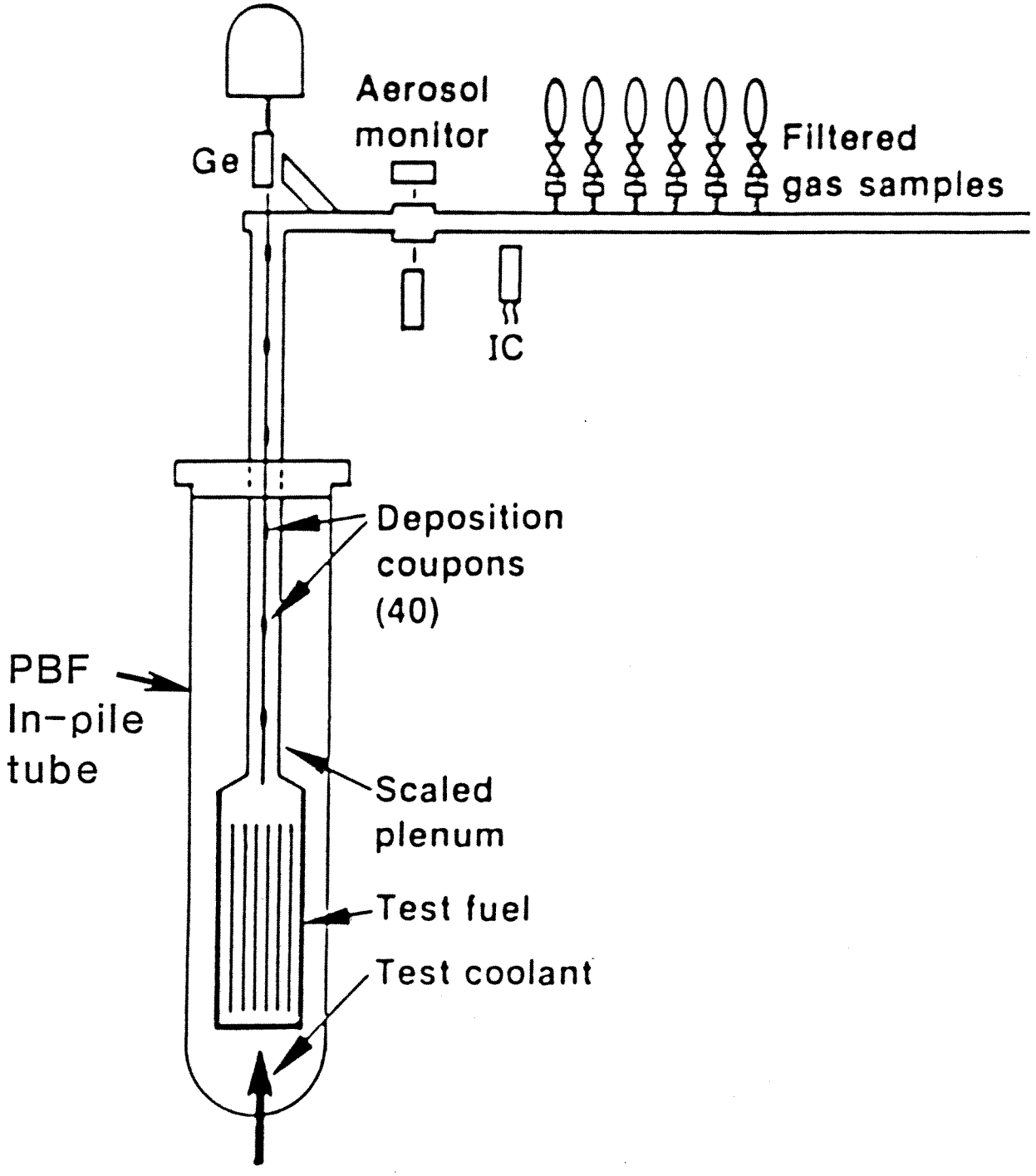

Figure 9. PBF SFD-14 Experiment

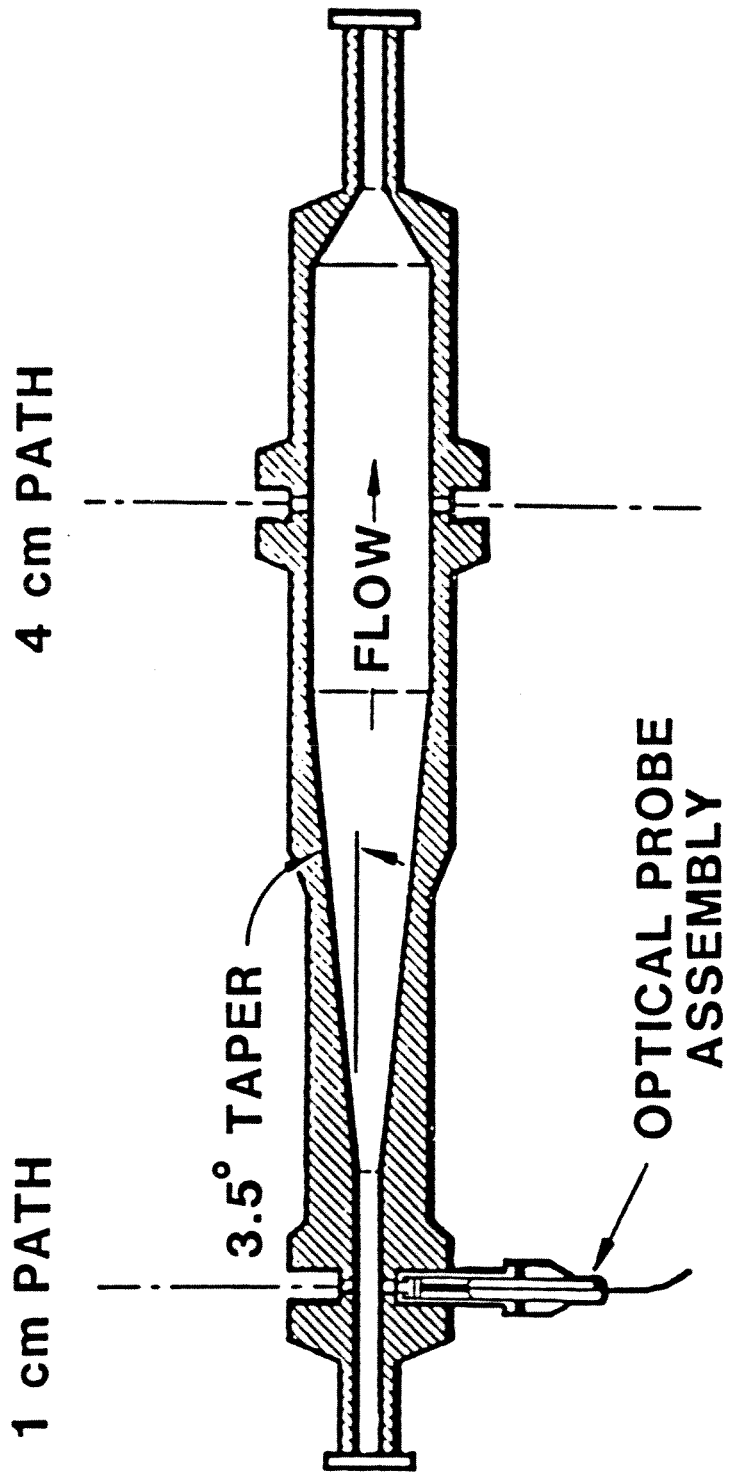

Figure 10. Dual Cell Extinction Monitor

The difference in number concentration is assumed to be due to only the coagulation process. As a result, the change in number concentration as a function of time for an aerosol undergoing coagulation is [Fuchs (1964)]:

$$dN/dt = 4\pi D_p D N^2[1+D_p(\pi Dt)^{-1/2}], \qquad (39)$$

where D is the diffusion coefficient for particle of diameter, D_p, and t the coagulation time in seconds.

Depending on experimental conditions, the second term in the bracket is usually less than 1 and considered negligible. The solution of the simplified form of Equation (39) is given by:

$$1/N_o = 1/N - kt, \qquad (40)$$

where N_o is the initial number concentration (particles/cm^{-3}), N the number concentration after time t (particles/cm^{-3}), and k the coagulation coefficient (cm^3/particles·s). The coagulation coefficient can be calculated for particles of a given size by:

$k = 4BTC/3\eta$,

B = Boltzman's constant = 1.38×10^{-16} erg/K,

T = temperature (K),

C = Cunningham slip correction factor, and

η = gas absolute viscosity (g/cm·s).

Based on the work of Gillespie (1963), Riest (1984) gives the following expression for the coagulation coefficient of log-normally distributed polydisperse aerosols:

$$k = 2BT[1+\exp(\ln^2 GSD) + 4.52[\exp(0.5 \ln^2 GSD) + \exp(2.5\ln^2 GSD]\lambda/D_p]/3\eta, \qquad (41)$$

where GSD is the geometric standard deviation of the particle size distribution and λ the mean free path of the gas molecules.

Changing from monodisperse to polydisperse aerosols does not alter Equation (40). The difference between the coagulation coefficients calculated by Equation (41) and that used in Equation (40) is less than 15% when $\lambda/d < 0.02$ and GSD < 1.5 In terms of the aerosol monitor, Equation (40) can be written with the initial concentration equal to the number concentration in the first cell, N, and the final concentration equal to the number concentration in the second cell, N':

$$N/N' = 1+ktN. \qquad (42)$$

Substituting into Equation (38):

$$\frac{L' \ell n[I/I_o]}{L \ell n[I'/I'_o]} = 1+ktN \qquad (43)$$

Because of the high temperatures and pressures encountered in PBF-type experiments, the Cunningham correction factor reduces to near unity for particle sizes greater than 0.1 μm. This, in turn, yields a constant coagulation coefficient, k. Because the path lengths are known, the intensity ratios are measured and the transit time is determined from flow rate measurements, Equation (43) can be immediately solved for N. The number concentration as a function of time is obtained directly from extinction measurements with no *a priori* knowledge of particle size or extinction coefficient history.

References

Adams, J.P., Partin, J.K., Petti, D.A., and Reed, T.R., "Development and Calibration of an Aerosol Monitor Used in the PBF SFD 1-4 Experiment", Proceedings of the 4th Miami International Symposium on Multiphase Transport and Particulate Phenomena, Miami Beach, Florida, December 1986.

Agarwal, J. K., and Liu B. Y. H., "A Criterion for Accurate Aerosol Sampling in Still Air", American Industrial Hygiene Journal, Vol.41, p. 191-197, 1980.

Albrecht, H., Matschoss, V., and Wild, H., "Investigation of Activity Release during Light Water Reactor Core Meltdown", p. 278-283, NUREG/CR-1724, 1980.

Ariessohn, P.C., Self, S. A., and Eustis, R. H., "Two Wavelength Laser Transmissometer for Measurements of the Mean Size and Concentration of Coal Ash Droplets in Combustion Flows", Applied Optics, p. 3775-3781, 1980.

Bachalo, W.D., and Houser, M.J., "Development of the Phase/Doppler Spray Analyzer for Liquid Drop Size and Velocity Characterizations", Paper No. AIAA-84-1199, AIAA/SAE/ASME 20th Joint Propulsion Conference, Cincinnati, OH, June 1984.

Baron, P.A., "Calibration and Use of the Aerodynamic Particle Sizer (APS 3300)", Aerosol Science and Technology, Vol. 5, p. 55-67, 1986.

Brewer, J. M., and Goren, S. L., "Evaluation of Metal Oxide Whiskers Grown on Screens for Use as Aerosol Filtration Media", Aerosol Science and Technology, Vol. 3, p. 411-429, 1984.

Brock, J.R., "On the Theory of Thermal Forces Acting on Aerosol Particles", J. Colloid Science, Vol. 17, p. 768-780, 1962.

Buescher, B. J., Osetek, D. J. and Ploger, S.A., "Power Burst Facility Severe Fuel Damage Test Series", EG&G Idaho, Inc. Paper No. EGG-M-083382, 1982.

Bunz, H., and Schock, W., "Measurements of the Condensation of Steam on Different Aerosols under LWR Core Melt Down Conditions", p. 171-180, NUREG/CR-1724, 1980.

Chen, C. Y., "Filtration of Aerosols by Fibrous Media", Chem. Rev., Vol. 5, p. 595-623, 1955.

Cheng, Y.S., and Yang, C.S., "Motion of Particles in Bends of Circular Pipes", Atmos. Environ., Vol. 15, p. 301-306, 1981.

Chyssler, J., Hesbol, R., Jansson, E., Piispaner, W., Sandstrom, R., and Strom,"Measurement System, Tests 1 and 2", Marviken Project Report MX5-34M, May 1983.

Crane, R. I., and Evans, R. L., "Inertial Deposition of Particles in a Bent Pipe", Journal of Aerosol Science, Vol. 8, p. 161-170, 1977.

Davies, C. N., "The Entry of Aerosols into Sampling Tubes and Heads", British J. Applied Physics Ser. 2, Vol. 1, p. 921-932, 1968.

Dunn, P. F., Herceg, J. E., and Johnson, C.E., "A Sampling System for the Physicochemical Characterization of Fission-Product Aerosols Formed During Light-Water-Reactor Experiments", Aerosol Science and Technology, Vol. 2, p. 257, 1983.

Elrick, R. M., "A First Study of Aerosols Produced by Neutronic Heating of Fresh UO_2 Fuel Under Core-Disruptive Accident Conditions", NUREG/CR-2296, October 1982.

Elrick, R. M., "A Time-Resolving Sampler to Determine Initial Fuel Aerosols Under CDA Conditions", p. 73-83, NUREG/CR-1724, 1980.

Fuchs, N. A., The Mechanics of Aerosols, Pergammon Press, New York, p. 264, 1964.

Gillespie, T., "The Effect of Size Distribution on the Rate Constants for Collisions in Disperse Systems", J. Colloid Science, Vol. 18, p. 562-567, 1963.

Herceg, J. E., Blomquist, C. A., Chung, K. S., Dunn, P. F., Johnson, C. E.,Kraft, D. A., Schlenger, B. J., Shaftman, D. H., and Simms, R., "TREAT Light Water Reactor Source Term Experiments Program", American Nuclear Society Topical Meeting, Fission Product Behavior & Source Term Research, Snowbird, Utah, July 15-19, 1984.

Heyder, J., Gebhart, J., and Scheuch, G., "Interaction of Diffusional andGravitational Particle Transport in Aerosols", Aerosol Science and Technology, Vol. 4, p. 315-326, 1985.

Himeno, Y. and Takahashi, J., "Sodium Mist Behavior in Cover Gas Space of LMFBR, Out-Pile Experiment", J. of Nuclear Science and Technology, p. 404-412, 1980.

Holve, D.J., "*In Situ* Measurements of Flyash Formation from Pulverized Coal", Combust. Sci. and Tech., Vol. 44, p. 269-288,1986.

Ingham, D.B., "Gravity Settling of Aerosol Particles in Horizontal Rectangular Tubes with Some Diffusion", Journal of Aerosol Science, Vol. 8, p. 139-147, 1977.

Ingham, D. B., "Diffusion of Aerosol From a Stream Flowing Through a Cylindrical Tube, Journal of Aerosol Science", Vol. 6, p. 125-132, 1975.

Kanapilly, G.M., Cheng, Y.S., Gray, R.H., and Yeh, H.C., "A Comparative Instrumental Study on the Size Characteristics of Yttrium Oxide Aggregate Aerosols", p. 302-317, NUREG/CR-1724, 1980.

Kirsch, A. A., and Stechkina, I. B., "The Theory of Aerosol Filtration with Fibrous Filters", Fundamentals of Aerosol Science, D. Shaw, Editor, John Wiley & Sons, New York, p. 165-256, 1978.

Lorenz, R. A., Hobson, D. O., and Parker, G. W., "Fuel Rod Failure Under Loss-of-Coolant Conditions in TREAT", Nuclear Technology, Vol. 11, p. 502-520, August 1971.

McPherson, G.D., and Hicks, D., "LOFT Goes out with a Severe Accident", Nuclear Engineering International, p. 24, April 1986.

Miller, R.W., Applehans, A.D., Bolstad, J.O., Courtright, E.L., Novick, V.J., Alvarez, J.L., and Deason, V.A., Instrument Development Summary Report for the Power Burst Facility Severe Fuel Damage Series 2, EG&G Report FIN No. A6305, March 1984.

Natanson, G. L., "Diffusion Precipitation of Aerosols on a Streamlined Cylinder with a Small Capture Coefficient", Dokl. Akad. Nauk USSR, Vol. 11, p. 100, 1957.

Novick, V. J., "The Use of Series Light Extinction Cells To Determine Aerosol Number Concentration", Aerosol Science and Technology - In Press, 1988.

Novick, V. J., and Alvarez, J. L. "Design of a Multistage Virtual Impactor", Aerosol Science and Technology, Vol. 6, p. 63-70, 1987.

Nuclear Aerosols in Reactor Safety, Nuclear Energy Agency, Organization for Economic Co-Operation and Development, June 1979.

Osetek, D.J., "Results of the Four Severe Fuel Damage Tests", NUREG/CP-0090, Fiftheenth Water Reactor Safety Information Meeting, Gaithersburg, Maryland, October 26-30, 1987.

Parker, G. W., "Experimental Techniques of the Characterization of Nuclear Aerosols", p. 278-301, NUREG/CR-1724, 1980.

Pui, D.Y.H., Romay-Novas, F., and Liu, B.Y.H., "Experimental Study of Particle Deposition in Bends of Circular Cross Section", Aerosol Science and Technology, Vol. 7, p. 301-315, 1987.

Riest, P.C., Introduction of Aerosol Science, MacMillan Publishing Company, New York, New York, p. 259, 1984.

Sauter, H. and Schutz, W., "Aerosol Release from a Hot Sodium Pool and Behavior in Sodium Vapor Atmosphere", p. 84-94, NUREG/CR-1724, 1980.

Schock, W., "Application of Optical Methods in Nuclear Aerosol Measurements", p. 221-231, NUREG/CR -1724, 1980.

Sem, G. J., and Daley, P. S., "Performance Evaluation of a New Piezoelectric Aerosol Sensor", Aerosol Measurement, D.A. Lundgren *et al.*, Editors, University Presses of Florida, p. 672-686, 1979.

Sinclair, D., Countess, R. J., Liu, B.Y.H., and Pui, D.Y.H., "Experimental Verification of Diffusion Battery Theory", APCA Journal, Vol. 26, p. 661-663, 1976.

Sinha, M. P., Griffin, C. E., Norris, D. D., and Friedlander, S. K., "Continuous Monitoring of Aerosols", p. 54, NASA Tech Brief, Vol. 7, No. 1, Item #40, Fall 1982.

Stechkina, I. B., and Fuchs, N. A., "Studies on Fibrous Aerosol Filters-I.Calculation of Diffusional Deposition of Aerosols in Fibrous Filters", Ann. Occup. Hyg., Vol. 9, p. 59-64, 1966.

Thomas, J.W.,"Gravity Settling of Particles in a Horizontal Tube", APCA Journal,Vol. 8, p.32-34, 1958.

Waldmann, L., and Schmitt, K. H., in Aerosol Science, C. N. Davies, Editor, Academic Press, London, p. 137-161, 1966.

Woods, D. C., "Measurement of Particulate Aerosol Mass Concentration Using Piezoelectric Crystal Microbalance", Aerosol Measurement, D.A. Lundgren *et al.*, Editors, University Presses of Florida, p. 119-130, 1979.

Wright, A.L., Kress, T.S., and Smith, A.M., "ORNL Experiments to Characterize Fuel Release from the Reactor Primary Containment in Severe LMFBR Accidents NUREG/CR-1724, 1980.

Yeh, H. C., "Use of Heat Transfer Analogy for a Mathematical Model of Respiratory Tract Deposition", Bulletin of Mathematical Biology, 36, No. 2, p. 105-116, 1976.